
This is an electronic reprint of the original article.
This reprint may differ from the original in pagination and typographic detail.

Väisänen, Saija; Ajdary, Rubina; Altgen, Michael; Nieminen, Kaarlo; Kesari, Kavindra K.;
Ruokolainen, Janne; Rojas, Orlando J.; Vuorinen, Tapani

Cellulose dissolution in aqueous NaOH–ZnO : cellulose reactivity and the role of ZnO

Published in:
Cellulose

DOI:
[10.1007/s10570-020-03621-9](https://doi.org/10.1007/s10570-020-03621-9)

Published: 01/02/2021

Document Version
Publisher's PDF, also known as Version of record

Published under the following license:
CC BY

Please cite the original version:
Väisänen, S., Ajdary, R., Altgen, M., Nieminen, K., Kesari, K. K., Ruokolainen, J., Rojas, O. J., & Vuorinen, T. (2021). Cellulose dissolution in aqueous NaOH–ZnO : cellulose reactivity and the role of ZnO. *Cellulose*, 28(3), 1267-1281. <https://doi.org/10.1007/s10570-020-03621-9>

This material is protected by copyright and other intellectual property rights, and duplication or sale of all or part of any of the repository collections is not permitted, except that material may be duplicated by you for your research use or educational purposes in electronic or print form. You must obtain permission for any other use. Electronic or print copies may not be offered, whether for sale or otherwise to anyone who is not an authorised user.



Cellulose dissolution in aqueous NaOH–ZnO: cellulose reactivity and the role of ZnO

Saija Väisänen · Rubina Ajdary · Michael Altgen · Kaarlo Nieminen · Kavindra K. Kesari · Janne Ruokolainen · Orlando J. Rojas · Tapani Vuorinen

Received: 3 June 2020 / Accepted: 12 December 2020 / Published online: 6 January 2021
© The Author(s) 2021

Abstract Cellulose utilization at its full potential often requires its dissolution which is challenging. Aqueous NaOH is the solvent of choice due to the rapid, non-toxic, low cost and environmentally friendly dissolution process. However, there are several limitations, such as the required low temperature and cellulose's moderately low degree of polymerization and concentration. Moreover, there is a tendency for gelation of semidilute solutions with time and temperature. The addition of ZnO aids cellulose dissolution and hinders self-aggregation in

the NaOH solution; however, the exact role of ZnO has remained as an open question. In this work, we studied cellulose dissolution in the aqueous NaOH–ZnO system as well as the reactivity of the dissolved cellulose by oxidation with 4-AcNH-TEMPO⁺ (TEMPO⁺). Based on Raman spectroscopic studies and the TEMPO⁺-reactivities, we propose a new structure for cellulose dissolved in aqueous NaOH–ZnO.

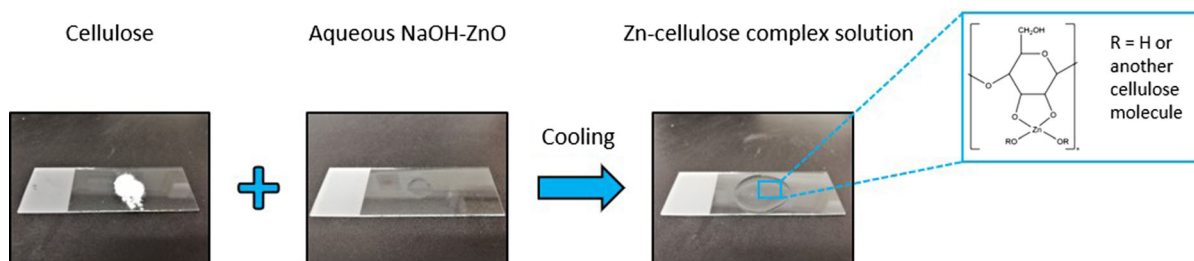
Supplementary Information The online version contains supplementary material available at <https://doi.org/10.1007/s10570-020-03621-9>.

S. Väisänen (✉) · R. Ajdary · M. Altgen · K. Nieminen · O. J. Rojas · T. Vuorinen
Department of Bioproducts and Biosystems, School of Chemical Engineering, Aalto University, P.O. Box 16300, 00076 Aalto, Finland
e-mail: saija.vaisanen@aalto.fi

K. K. Kesari · J. Ruokolainen
Department of Applied Physics, School of Science, Aalto University, P. O. Box 15100, 00076 Aalto, Finland

O. J. Rojas
Departments of Chemical and Biological Engineering, Chemistry, and Wood Science, Bioproducts Institute, The University of British Columbia, 2360 East Mall, Vancouver BC V6T 1Z3, Canada

Graphic abstract



Keywords Cellulose · Dissolution · Reactivity · Raman spectroscopy · TEMPO-oxidation · UV/Vis-spectroscopy

Introduction

Cellulose is a versatile raw material which can be converted into numerous products applicable in various fields. However, its full potential is not fully met, partly due to the difficulty in dissolving it. Cellulose dissolution is a prerequisite for manufacturing value-added cellulosic products, such as regenerated fibers, filaments and films (Wawro et al. 2009; Yang et al. 2011a), and producing functional cellulose-based materials in a homogenous environment (Gericke et al. 2013; Wang et al. 2016). Functionalizing cellulose in the dissolved state is desired due to the full availability of hydroxyl (OH) groups, control of both the degree of substitution (DS) and the distribution of the functional groups as well as minimal chain degradation and high yield due to small consumption of reagent by side reactions (Heinze et al. 2000). Yet, as the load-bearing structure in nature, cellulose is a recalcitrant polysaccharide organized in the plant cell wall in a hierarchical structure that resists degradation. The stiffness of cellulose chains and their close packing through numerous hydrogen bonds make dissolving cellulose difficult. Cellulose solubility is affected by strong intra- and intermolecular hydrogen bonding as well as hydrophobic interactions between the molecules (Lindman et al. 2010; Medronho and Lindman 2015). Therefore, it is insoluble in water and in the most common organic solvents.

Cellulose can, however, be dissolved with certain solvents or solvent systems which are able to diffuse in and disrupt the crystalline structure as well as

dissociate cellulose chains from each other (Ghasemi et al. 2017a, b). Cellulose dissolution typically begins with swelling of the fibers. When cellulose is placed in contact with a solvent, the solvent molecules permeate into the structure of the biopolymer changing its volume and physical properties (Medronho and Lindman 2015). If the cellulose-solvent interactions are stronger than the intra- and intermolecular interactions between cellulose chains, the crystalline network of cellulose is gradually destroyed increasing the possibility of conformational chain movement of individual chains (Rabideau et al. 2013). The weakening interactions between cellulose molecules and the increasing chain movement result in the transformation of solid cellulose fibers to swollen gel-like medium (Ghasemi et al. 2017a; Lu et al. 2011). With increasing swelling, the individual cellulose chains start to disintegrate from each other and diffuse into the bulk solution (Ghasemi et al. 2017a). In complete dissolution, the supramolecular structure of cellulose is expected to be completely destroyed resulting in a solution where cellulose chains are separated from each other. Generally, dissolution is favored by an increase of entropy in solution (e.g. the entropy of mixing and the entropy of conformation mobility) and thus, due to the long polymer chains, dissolving polymers is more challenging than dissolving their parent monomers (Budtova and Navard 2016). The former is true also for cellulose. However, the dissolution of cellulose is additionally hindered by two properties, namely, (1) the rigidity of cellulose chains limiting the degrees of freedom when the chain is dissolving and (2) the tendency of cellulose molecules to self-aggregate in solution (Budtova and Navard 2016). Thus, a good cellulose solvent is not only able to disturb the interaction between cellulose chains but also to prevent them from self-aggregating in solution.

Aqueous sodium hydroxide solution is a promising choice for cellulose dissolution due to the rapid, non-toxic, low cost and environmentally friendly dissolution process. The process for dissolving cellulose in aqueous NaOH was discovered already in the early 1900s (Davidson 1934, 1936) and it is still attracting a lot of interest (Cai et al. 2008; Egal et al. 2007; Hagman et al. 2017; Huh et al. 2020; Medronho and Lindman 2015). Cellulose dissolves rapidly in aqueous NaOH, however, the dissolution is limited to low temperatures ($< 0\text{ }^{\circ}\text{C}$), moderately low degree of polymerization (DP), low concentration of cellulose and narrow concentration range of NaOH (7–10%) (Budtova and Navard 2016; Cai et al. 2008; Egal et al. 2007; Hagman et al. 2017; Isogai and Atalla 1998; Medronho and Lindman 2015). Furthermore, there is a tendency for gelation of semidilute solutions (e.g. 5% cellulose in 9% NaOH solution) with increased time and temperature (Liu et al. 2011; Pereira et al. 2018; Roy et al. 2003). One of the leading theories explaining cellulose dissolution in aqueous NaOH at low temperature is the formation of hydrates with water that permeate into the structure of the cellulosic material and detach individual chains from each other (Cai et al. 2008; Egal et al. 2007). According to Egal et al. (2007) the structure of aqueous NaOH–cellulose solution is highly dependent on the concentrations of the species present in the solution and at the optimal concentrations, there is an unstable equilibrium between NaOH hydrates bonded to each other and to cellulose. On the other hand, charging up polymers is expected to increase their solubility. In the strongly alkaline conditions typically used for cellulose dissolution, cellulose is in a dissociated form which can play a significant role in the dissolution of this polymer (Kihlman et al. 2013). This phenomenon was studied by Bialik et al. (2016) who have shown that there is a correlation between the dissolving power of alkali hydroxides and their pK values. As possible explanations for the counter-intuitive effect of temperature to cellulose dissolution in aqueous NaOH, it has been proposed that the network of NaOH hydrates is stronger at low temperatures preventing cellulose chains from interacting with each other (Egal et al. 2007). Alternatively, more polar conformations of cellulose are favored at low temperature promoting interactions with the polar solvent (Medronho and Lindman 2014).

The dissolution of cellulose in aqueous NaOH and the stability of the solution against gelation can be enhanced with certain additives, such as a small amount of zinc oxide (Kihlman et al. 2013; Liu et al. 2011; Yang et al. 2011b). Despite active research, the role of ZnO has remained to be an open question. ZnO forms zincate ($\text{Zn}(\text{OH})_4^{2-}$) in strongly alkaline solution, and it has been suggested that this species enhances the dissolution of cellulose by forming even stronger hydrogen bonds with it (Yang et al. 2011b). On the other hand it has also been suggested that $\text{Zn}(\text{OH})_4^{2-}$ enhances cellulose dissolution by associating to it and thus further charging up the molecules in the alkaline conditions (Kihlman et al. 2013). Moreover, Liu et al. (2011) have suggested that ZnO acts as water “binder” stabilizing cellulose solutions in aqueous NaOH.

The work presented here contributes to the understanding of cellulose dissolution in aqueous NaOH–ZnO and elaborates on the role of ZnO. Moreover, the reactivity of cellulose dissolved in the NaOH–ZnO system is discussed. Two samples, microcrystalline cellulose consisting of pure, low molecular weight cellulose and never-dried, bleached softwood pulp containing cellulose of high molecular weight were dissolved in a solvent system containing 9 w-% NaOH and 1 w-% ZnO. The structure of the samples was studied with Raman spectroscopy and the reactivities were assessed based on oxidation with 4-acetamido-2,2,6,6-tetramethylpiperidine-1-oxo-piperidinium cation (4-AcNH-TEMPO⁺) as a probe reaction with the method published by Khanjani et al. (2017). 2,2,6,6-tetramethylpiperidine-1-oxyl radical (TEMPO) -catalyzed oxidation in alkaline pH has been widely studied in the production of oxidized cellulose nanofibrils because of the high reaction rate, yield and selectivity (Isogai et al. 2011; Okita et al. 2010; Saito et al. 2007, 2009; Salminen et al. 2017). The actual oxidizing agent in these reactions is the TEMPO⁺-cation (Isogai et al. 2011). It is able to rapidly and selectively convert the hydroxymethyl groups of cellulose into carboxylate groups in mild conditions (pH 9, room temperature) (De Nooy et al. 1994). In addition, the reaction can be followed and quantified with iodometry (Bichsel and von Gunten 1999; Pääkkönen et al. 2015; Khanjani et al. 2017). Thus, oxidation with 4-AcNH-TEMPO⁺ provides a means to study cellulose reactivity quantitatively. Raman spectroscopy was chosen for the structural

studies as it enables analysis of chemical bonds at the molecular level. Moreover, it is non-destructive and enables analysis of samples in their native state since minimal sample preparation is required and also wet samples can be analyzed (Agarwal 2014). Raman spectroscopy is especially useful in studying cellulosic samples as, in general, the materials are inherently not fluorescent and thus the obtained Raman spectra have good signal-to-noise ratios (Agarwal 2019). In the current work, oxidation with 4-AcNH-TEMPO⁺ as a means to study the reactivity of cellulose in the dissolved state is reported for the first time, and, based on the reactivity studies as well as the Raman spectroscopic analyses, a new structure for cellulose dissolved in aqueous NaOH–ZnO is proposed.

Materials and methods

Materials

The samples were never-dried bleached softwood (SW) kraft pulp obtained from UPM-Kymmene Oyj and microcrystalline cellulose powder (MCC; Avicel, PH-101, ~ 50 µm particle size) obtained from Sigma-Aldrich, Ireland. In addition, cellohexaose (purity > 90%) from Megazyme International, Ireland as well as amorphous cellulose (AC) prepared from the MCC with a method modified from Mormann and Wezstein (2009) were studied as references with Raman spectroscopy. In preparing the amorphous cellulose, 3 mol of hexamethyldisilazane (HMDS) was used per anhydroglucose unit (AGU) for the silylation and the reaction medium was EmimAc with 10% MCC concentration. Desilylation was done in a slightly acidic water reflux.

For the molecular weight distribution analyses, the samples were dissolved in LiCl/DMAc solution which was prepared from LiCl (purity > 98.5%) purchased from VWR Chemicals and DMAc (HPLC-grade) from VWR Chemicals. NaOH (purity 99.6%) from VWR Chemicals and ZnO (pro analysis) from Merck were used for preparing the cellulose solvent. For the TEMPO-oxidation studies, 4-acetamido-2,2,6,6-tetramethylpiperidine-1-oxo-piperidium (4-AcNH-TEMPO⁺) tetrafluoroborate (purity 97%) and pH 2 buffer solution (AVS titrinorm) were purchased from Sigma-Aldrich and VWR Chemicals, respectively. Boric acid (purity > 99.8%) from Sigma Aldrich and

NaOH (purity 99.6%) from VWR Chemicals were used to prepare the pH 9 buffer solution for the oxidation experiments. All dilutions were done in Milli-Q water (Millipore Corporation, resistivity 18.2 MΩ cm).

Structural characterization of the samples

The samples were characterized for their dry matter (DM) and structural carbohydrate contents as well as their DP_w (Table 1). The dry matter contents were determined according to the standard ISO 638:1978 and the structural carbohydrate contents were analyzed according to the analytical method NREL/TP-510-42618 published by the U.S. National Renewable Energy Laboratory (NREL) (Sluiter et al. 2008). For the structural carbohydrate contents determination, the samples were acid-hydrolyzed to their constituent monosaccharides and analyzed with high-performance anion-exchange chromatography with pulsed amperometric detection (HPAEC-PAD) with a Dionex ICS-3000 system (Thermo Fisher Scientific). The samples were studied in duplicate and two chromatography injections were done for each analysis. Based on the amounts of monosaccharides, the cellulose and hemicellulose contents were calculated according to the formula published by Janson (1970).

The DP_w of the samples was calculated from their molecular weight distributions that were analyzed from their solution in LiCl/DMAc with gel permeation chromatography (GPC) based on the method described in Borrega et al. (2013). To facilitate dissolution, the samples were first activated in Milli-Q water and then dehydrated by solvent-exchange with acetone. Prior to the dissolution, the samples were activated in DMAc overnight. Then the samples were dissolved in 90 mg/l LiCl/DMAc solution at room temperature under continuous mixing with a magnetic stirrer. The dissolved samples were diluted 10 times and analyzed with a Dionex UltiMate 3000 system (Thermo Fisher Scientific) with RI-detection (Shodex RI-101) coupled with multi angle laser light scattering (Viscotek SEC-MALS 20). Solution containing 9 g/l LiCl/DMAc was used as the eluent, two injections were performed for each analysis and pullulan standards (343 Da–708 kDa, Polymer Standard Service, and 2350 kDa, Fluka) were used to calibrate the system.

Table 1 Structural characterization of the cellulosic samples

Sample	DM (%)	DP _w	Component (% dry weight)		
			Cellulose	Xylan	Glucomannan
MCC	96	400	96	2	2
SW pulp	18	3680	83	9	8

The dissolution procedure

4 w-% of cellulosic sample (in dry matter) was dissolved in the solvent system containing 9 w-% NaOH and 1 w-% ZnO. The amounts of NaOH and ZnO were chosen based on previously published studies (Budtova and Navard 2016; Cai et al. 2008; Egal et al. 2007; Hagman et al. 2017; Isogai and Atalla 1998; Kihlman et al. 2013; Liu et al. 2011; Yang et al. 2011b) as well as preliminary studies optimizing the conditions for the system applied in the current work. First, NaOH and ZnO were dissolved in boiling water in the mass ratio of 6:1 (18 w-% in total) in order to dissolve ZnO and then cooled down to -10 °C. The cellulosic samples were activated in Milli-Q water in a separate container and then poured to the NaOH–ZnO solution while mixing with a mechanical stirrer in a salt-ice bath at -10 °C. For the Raman spectroscopic studies, the following additional references were prepared: 4 w-% cellohexaose in water, 4 w-% cellohexaose in NaOH–ZnO as well as pure NaOH–ZnO solvent. The amounts of NaOH and ZnO were 9 w-% and 1 w-%, respectively.

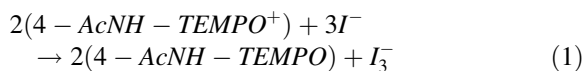
Optical and scanning electron microscopy imaging

The MCC and pulp samples were imaged with a Leica ICC50 HD microscope in their as-received state as well as immediately after their dissolution in the NaOH–ZnO system. In addition, the samples were imaged with scanning electron microscopy (SEM) before and after their dissolution. The never-dried pulp as well as the dissolved samples needed to be dried for the SEM study while the MCC was a dry powder and needed no sample preparation. The pulp was dried with critical point drying (CPD) in order to preserve its pore structure and the dissolved samples were vacuum dried. For the CPD, a method modified from Lovikka et al. (2016) was used. The pulp samples were placed into regenerated cellulose membrane tubings and solvent exchanged by dialysis into acetone for 48 h. Then, the samples were moved into a Leica EM

CPD300 critical point drier where the acetone was exchanged to liquid CO₂ over 18 cycles (ca. 2 h). In order to bring the CO₂ to its supercritical state, the system was heated to 35 °C under ca. 75 bar pressure. The samples were prepared for the SEM analysis in a low humidity room (< 10% RH). The CPD dried pulp and MCC were gently mounted onto a double-sided conductive carbon tape. The dissolved samples were dried directly on the carbon tape. Prior to the imaging, the samples were sputtered with iridium for 60–90 s by applying 30 mA current to form a 3–9 nm layer on the sample surface. The images were taken with a Zeiss Sigma VP SEM using a secondary electron detector at the accelerating voltage of 2.5–2.8 keV.

Oxidation with 4-AcNH-TEMPO⁺

The reactivity of the samples was studied with the method published earlier (Khanjani et al. 2017). The samples were oxidized with 4-AcNH-TEMPO⁺ which oxidizes hydroxymethyl groups to carboxylate groups (De Nooy et al. 1994). The reactions were done at room temperature in pH 9 buffer solution under continuous mixing. The consumption of 4-AcNH-TEMPO⁺ was monitored by its reaction with potassium iodide (KI) (Pääkkönen et al. 2015). The reaction between 4-AcNH-TEMPO⁺ and I[−] is shown in Eq. 1.



The formed I₃[−] was quantified by absorption spectrophotometry at the absorption maximum of I₃[−] at 288 nm (Bichsel and von Gunten 1999).

The total volume in each experiment was 100 ml and the amount of 4-AcNH-TEMPO⁺ was 2.5 mmol/l. The samples were studied in their as-received state as well as immediately after their dissolution in the NaOH–ZnO system. The amount of undissolved sample in each experiment was 0.5 g/l (in dry matter) while the amount of dissolved sample was 0.5 g/l, 0.1 g/l or 0.05 g/l (in dry matter) depending on the experiment. Prior to the oxidation, the undissolved

samples were ultrasonicated in the pH 9 buffer solution to achieve an even dispersion of the sample. For monitoring the consumption of 4-AcNH-TEMPO⁺, samples of the reaction solution (1 ml each) were mixed with 1 ml of a 10% KI and diluted to 40 ml with a pH 2 buffer solution. The absorption spectrum of the resultant solution was recorded at appropriate time intervals. The recording of time started at the time when 4-AcNH-TEMPO⁺ was mixed with the sample.

The values for reactivity (mmol/g) were obtained by nonlinear fitting of the oxidant decay data according to Eq. 2.

$$c = c_0 - 2\alpha + \alpha e^{-k_1 t} + \alpha e^{-k_2 t}, \quad (2)$$

where the c_0 and c refer to the concentration of 4-AcNH-TEMPO⁺ after the reaction time 0 (2.5 mmol/l) and t , respectively. The k_1 and k_2 are first-order rate constants for the oxidation of primary and secondary hydroxyl groups, respectively, and α is the fraction of 4-AcNH-TEMPO⁺ that reacts with the accessible hydroxyl groups of cellulose.

Raman spectroscopy

The Raman spectra of the samples were acquired as such except for the never-dried pulp, which was dried in the oven at 40 °C prior to the measurement. The dissolved samples were studied immediately after their dissolution. The Raman spectra were acquired using a WITec alpha 300 RA confocal Raman microscope equipped with a 532 nm frequency-doubled Nd:YAG laser (used at 30 mW), a 20 × air objective (NA = 0.4), and a DU970-BV EMCCD camera behind a 600 lines mm⁻¹ grating. An integration time of 0.5 s was used and the number of accumulations was 10 except for the dissolved MCC for which the number of accumulations was 50. Spectral analysis was done with the WITec ProjectPlus software. All spectra were baseline corrected by fitting a fifth-order polynomial and normalized on the band at ca. 1096 cm⁻¹.

Results and discussion

Cellulose dissolution in the NaOH–ZnO system

Figure 1 shows optical microscope images of the MCC and never-dried bleached SW pulp in their as-received state as well as after dissolving them in the NaOH–ZnO system including photos of the samples as inlays on the microscope images. Although, based on solely microscope imaging, it is not possible to distinguish between complete dissolution of cellulose and the formation of a fine dispersion, it is a quick and indicative way to estimate the dissolution capacity of the solvent. The MCC formed a clear liquid when dissolved in the NaOH–ZnO solvent system, and according to the microscopy image in Fig. 1c, there were only few small solid particles visible. These particles might be undissolved ZnO or small aggregates of cellulose. Similar small particles were visible also in the microscope image taken of the pure NaOH–ZnO solvent (Fig. S1d in the Supplementary Material). Hagman et al. (2017) have previously reported clusters of cellulose with an apparent size of > 1 μm in their study of MCC dissolved in aqueous NaOH. However, it is important to note that the samples were allowed to warm up to room temperature, the storage time at room temperature prior to the measurement was not mentioned and no ZnO was added to the system. Figure 1b shows the SW pulp fibers in their as-received state, and the fibers after the completion of the dissolution procedure are shown in Fig. 1d. The pulp formed an opaque gel in NaOH–ZnO, and in the microscope image (Fig. 1d) swollen fibers are visible. It is clear that the dissolution of the SW pulp in the NaOH–ZnO system was poor. Indeed, dissolving the SW pulp fibers with such a high DP (DP_w = 3680, Table 1) is not an easy task. The DP_w of the SW pulps was measured to be almost 10 times that of the MCC (DP_w = 400, Table 1). In fact, the main characteristic of cellulose influencing its dissolution in NaOH has been concluded to be its molecular weight (Isogai and Atalla 1998). Moreover, Young et al. (2011b) found that the solubility of cellulose in NaOH/urea/ZnO solution decreases linearly with increasing molecular weight of cellulose.

Figure 2 shows SEM micrographs of the samples. The surface of the MCC in NaOH–ZnO is covered with small, needle-like particles (Fig. 2c) whose size is estimated with a larger magnification (Fig. 2S in the

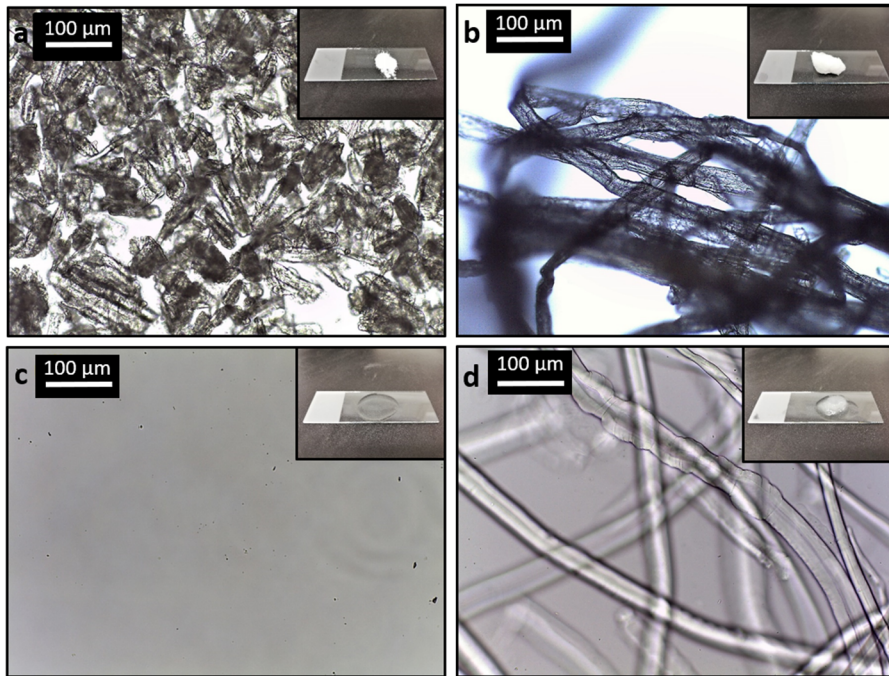


Fig. 1 Microscope images of the samples: **a** MCC, **b** never-dried SW pulp, **c** MCC in NaOH–ZnO and **d** never-dried SW pulp in NaOH–ZnO. Photos of the samples are included as inlays

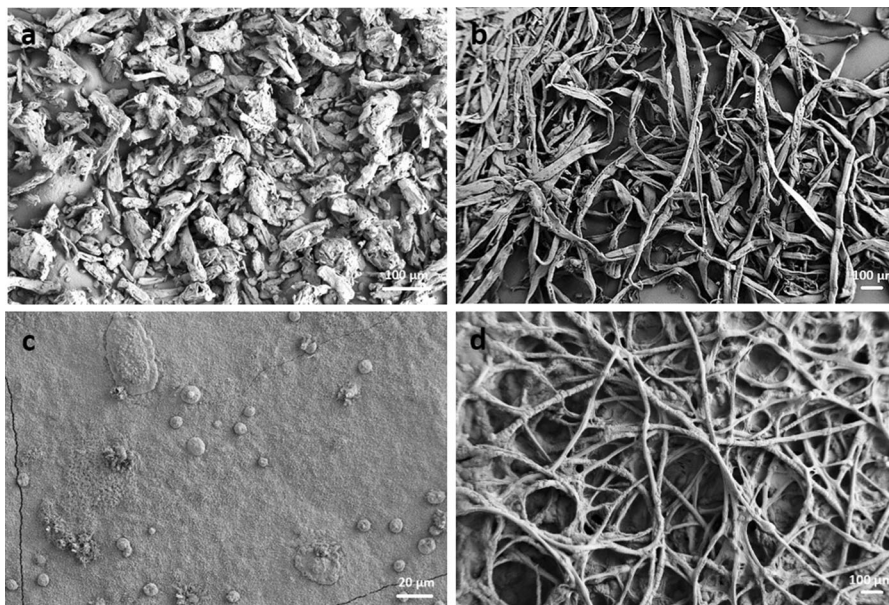


Fig. 2 SEM images of the cellulose samples: **a** MCC, **b** SW pulp, **c** MCC in NaOH–ZnO and **d** SW pulp in NaOH–ZnO

Supplementary Material) to be a few micrometers in length and a few hundred nanometers in width. Comparing the images in Fig. 2a, c, it is clear that the shape and size of these needle-like particles is very

different from those ones of the MCC prior to the dissolution. Thus, it is possible that these particles are formed by cellulose that was originally dissolved and has been aggregated when the sample was dried for the

SEM imaging. Alves et al. (2016) have previously reported similar needle-like particles in SEM micrographs taken for MCC in NaOH. These types of particles were not observed for the pulp in NaOH–ZnO (Fig. 2d). Besides the needle-like particles, there are also larger particles visible in both Fig. 2c, d. They might be undissolved ZnO, aggregates of the solvent and/or fractions of dissolved and aggregated cellulose. Energy-dispersive X-ray analysis (EDS) could not verify the chemical composition of these particles. Moreover, the image taken of the SW pulp after its dissolution in the NaOH–ZnO system shows undissolved fibers (Fig. 2d). A careful comparison of Fig. 2b, d reveals that the average width of the fibers after the NaOH–ZnO treatment (Fig. 2d) is smaller than the average width of the fibers that have undergone no dissolution procedure (Fig. 2b). This might suggest that the SW pulp fibers have partially dissolved during the dissolution procedure and, thus, the fibers in the SEM micrograph (Fig. 2d) are thinner. However, such conclusion cannot be made solely based on SEM imaging and further evidence for this is needed.

TEMPO⁺-reactivity

Figure 3a–c show UV–vis absorption spectra for the iodometric analysis of 4-AcNH-TEMPO⁺ from its reaction mixture with MCC dissolved in the NaOH–ZnO system and Fig. 3d–f show the consumption of 4-AcNH-TEMPO⁺ during oxidation of the dissolved MCC calculated based on the absorption spectra. To visualize how the consumption of 4-AcNH-TEMPO⁺ depends on the concentration of cellulose, three cases with varying cellulose concentration are shown. The amount of 4-AcNH-TEMPO⁺ in each experiment was the same (2.5 mmol/l) while the amount of MCC was 0.5 g/l, 0.1 g/l and 0.05 g/l (in dry matter) depending on the experiment.

In Fig. 3a, d, the relative amounts of 4-AcNH-TEMPO⁺ and MCC were chosen to be the same as what was found optimal in our previous work reporting TEMPO⁺-reactivity of undissolved cellulose samples (Khanjani et al. 2017). However, in the case of MCC dissolved in the NaOH–ZnO system, 4-AcNH-TEMPO⁺ reacts extremely fast and all 4-AcNH-TEMPO⁺ is consumed in the beginning of the reaction (Fig. 3a, d). When the amount of MCC is decreased to 0.1 g/l, a small absorption peak of I₃⁻ at

288 nm appears visible in the beginning of the reaction (Fig. 3b) showing that most of 4-AcNH-TEMPO⁺ is also consumed immediately in the beginning of the reaction. In contrast, the rest is consumed fast, within ca. 2 min since the beginning of the reaction (Fig. 3d). When the amount of MCC is decreased even more, to 0.05 g/l, the consumption of 4-AcNH-TEMPO⁺ becomes traceable (Fig. 3c, f). Also in this case, the most amount of 4-AcNH-TEMPO⁺ is consumed immediately in the beginning of the reaction. Some 4-AcNH-TEMPO⁺, however, is consumed at a slower rate and the consumption can thus be followed.

Figure 4 shows the consumption of 4-AcNH-TEMPO⁺ during the oxidation of MCC and the SW pulp in their as-received state as well as after their dissolution in the NaOH–ZnO system. The graph for the dissolved MCC (0.05 g/l) is shown here again for convenience. The solid line in the graphs represents the computational fit of the data according to the two-component first-order reaction system (Eq. 2) and the dotted and dashed lines are the fast and slow components of the reaction system, respectively. As observed from Fig. 4, the non-linear, two-component reaction system models the experimental data reasonably well for all of the samples. The oxidation of the cellulosic samples includes a faster, initially dominating reaction and a slower, more persisting reaction. The fast oxidation of hydroxymethyl groups of the MCC proceeds to the end within ca. 15 min (Fig. 4a) while the fast oxidation takes only ca. 5 min for the SW pulp (Fig. 4b). Furthermore, the initial reaction rate and the extent of overall reaction are higher for the SW pulp as compared to the MCC. The MCC consists of almost purely of cellulose while the SW pulp contains also hemicelluloses. This affects the consumption of 4-AcNH-TEMPO⁺ of the SW pulp as the hydroxymethyl groups of glucomannan in addition to cellulose may be oxidized by 4-AcNH-TEMPO⁺. Moreover, the structure of the MCC is highly crystalline while the SW pulp contains also non-ordered domains. It has been shown that the carboxylate groups formed by TEMPO-mediated oxidation are selectively present on cellulose crystallite surfaces (Saito et al. 2009). Thus, it is not surprising that the extent of the overall reaction of the SW pulp is found to be higher than that of the MCC.

As discussed before, and as seen in Fig. 4, the samples dissolved in the NaOH–ZnO system show

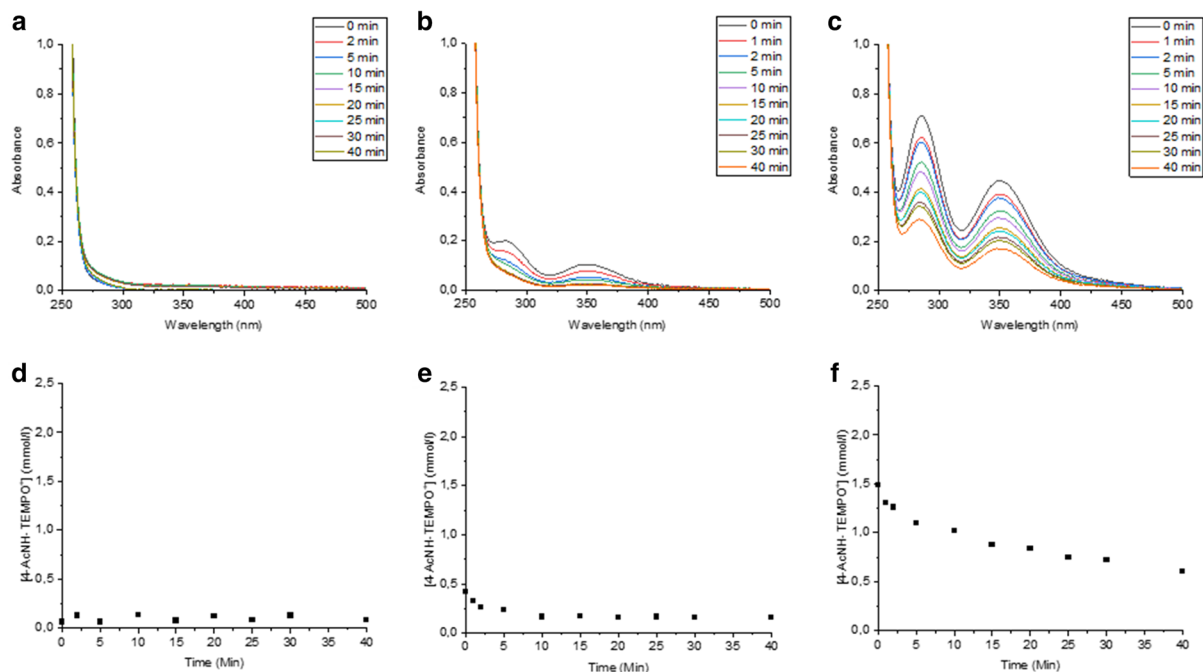


Fig. 3 UV-Vis absorption spectra of 4-AcNH-TEMPO⁺ and MCC in NaOH-ZnO with **a** 0.5 g/l MCC, **b** 0.1 g/l MCC, **c** 0.05 g/l MCC and the consumption of 4-AcNH-TEMPO⁺

during the oxidation of MCC in NaOH-ZnO with **d** 0.5 g/l MCC, **e** 0.1 g/l MCC and **f** 0.05 g/l MCC

significantly higher reactivities and initial reaction rates as compared to the samples prior to their dissolution. The fast oxidation of the hydroxymethyl groups proceeds to the end almost instantly for the MCC dissolved in NaOH-ZnO (Fig. 4c) and within ca. 2.5 min for the SW pulp in NaOH-ZnO (Fig. 4d). In our previous work, we have shown for 1-propanol and maltose that mixing 4-AcNH-TEMPO⁺ with hydroxymethyl-containing species in dissolved state leads immediately to complete oxidation of the hydroxymethyl groups based on the stoichiometry of the reactions (Khanjani et al. 2017). It can be assumed that the same is true for the MCC dissolved in aqueous NaOH-ZnO and the immediate reaction observed for this sample consists solely of oxidation of hydroxymethyl groups in dissolved form.

The computational fitting of the experimental data in Fig. 4 makes it possible to quantify the extent of the fast oxidation and thus the reactivities (contents of carboxylate groups introduced by 4-AcNH-TEMPO⁺) and the computational degree of oxidation of hexopyranosyl units by 4-AcNH-TEMPO⁺. The reactivities of the undissolved MCC and SW pulp are 0.58 mmol/g for both of the samples corresponding to the

computational degree of oxidation of 9.5% for the MCC and 10.4% for the SW pulp when the carbohydrate composition of the samples is taken into account. The reactivities of the MCC and SW pulp dissolved in the NaOH-ZnO system are 5.92 and 4.69 mmol/g, respectively, corresponding to the degrees of oxidation of 97.9% and 83.8%. Thus, it seems that essentially all hydroxymethyl groups of the MCC in NaOH-ZnO are oxidized by 4-AcNH-TEMPO⁺ immediately when the sample is mixed 4-AcNH-TEMPO⁺ indicating that cellulose has fully dissolved, i.e. is in molecularly dispersed form, in the NaOH-ZnO system. Moreover, the reactivity of the SW pulp is increased by ca. 73%-points by the NaOH-ZnO treatment.

Finally, it is important to note that cellulose dissolved in the NaOH-ZnO system is expected to start recrystallizing when the 4-AcNH-TEMPO⁺ aqueous solution is introduced to the system. The high degree of oxidation of the hydroxymethyl groups of the MCC in NaOH-ZnO clearly shows that the rapid oxidation reaction proceeds to the end before cellulose in the solution starts recrystallizing. We have also studied MCC dissolved in two other systems,

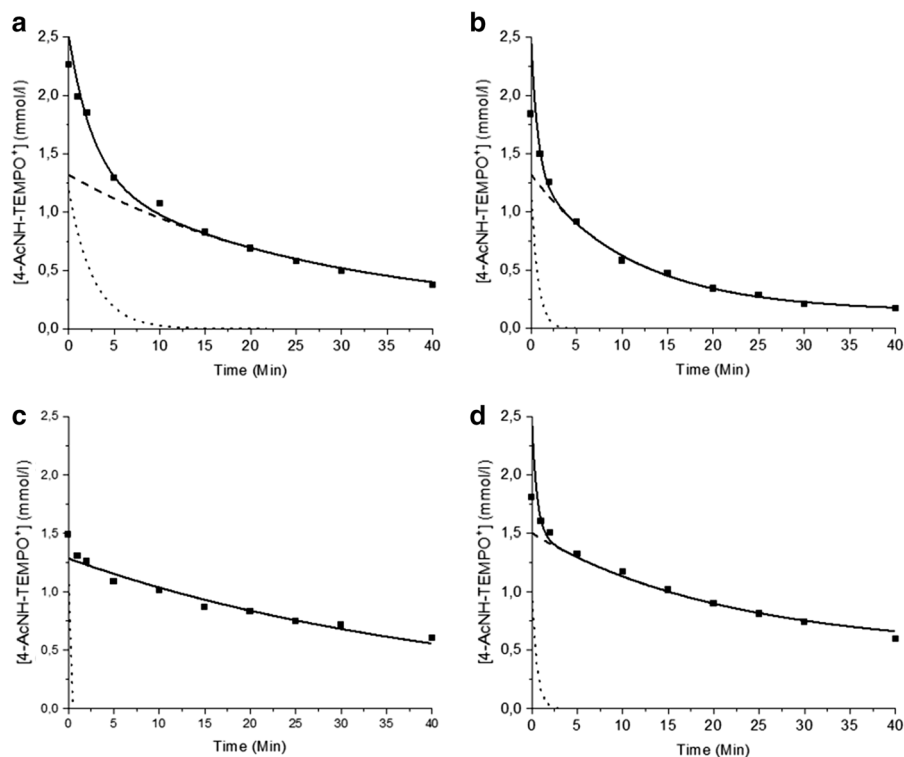


Fig. 4 Consumption of 4-AcNH-TEMPO⁺ during oxidation of 0.5 g/l MCC (a) and SW pulp (b), and 0.05 g/l MCC (c) and SW pulp (d) in NaOH–ZnO. The fast and slow components of the fit (solid line) are represented by dotted and dashed lines, respectively

namely LiCl/DMAc and 1-ethyl-3-methylimidazolium acetate ([Emim][Ac]), and the same was not observed for these systems (figure S3 in the Supplementary Material). In these solvents, the consumption of 4-AcNH-TEMPO⁺ stopped during the experiment and the total consumption of 4-AcNH-TEMPO⁺ was markedly smaller than for the samples dissolved in the NaOH–ZnO system showing that 4-AcNH-TEMPO⁺ was unable to oxidize all the hydroxymethyl groups of cellulose dissolved in LiCl/DMAc and [Emim][Ac]. This is most probably due to rapid recrystallization of cellulose when water was introduced to the system. The concentration of cellulose at the point of precipitation in the solution-coagulant interface is very high, thus favoring the formation of a dense cellulose “skin” (Medronho and Lindman 2015). Rapid regeneration of cellulose on the surface of the solution markedly hinders the reaction between cellulose and 4-AcNH-TEMPO⁺. The fact that the same is not observed for cellulose in the NaOH–ZnO solvent system indicates that rapid recrystallization is not happening in this system. Thus, there must be

something in the system that impedes rapid recrystallization of cellulose when water is added and the cellulose hydroxymethyl groups are able to react with 4-AcNH-TEMPO⁺. Let us elaborate this further in the next section.

Raman spectroscopy

The state of cellulose in the NaOH–ZnO solvent system and the solvent-cellulose interactions were studied with Raman spectroscopy. Raman spectroscopy is a useful tool to study the composition and structure of cellulosic materials as it provides information at the molecular level. Changes in the local molecular environments are reflected in changes in the intensities, positions and shapes of the Raman bands. In general, highly ordered and crystalline materials produce sharp and intense bands while the bands of unordered structures are broader and less intense (Agarwal and Ralph 1997). As highly ordered and crystalline polymer, the Raman bands of cellulose are sharp and intense, and, due to numerous studies

over the years, they are well known (Agarwal 2014; Agarwal and Ralph 1997; Blackwell et al. 1970; Eronen et al. 2009; Schenzel and Fischer 2001; Wiley and Atalla 1987). Most of the Raman features characteristic of cellulose are found in the fingerprint region between 250 and 1500 cm^{-1} .

Figure 5 shows the Raman spectra in the region of 300–1500 cm^{-1} for the MCC (Fig. 5a) and the SW pulp (Fig. 5b) prior to their dissolution in the NaOH–ZnO system as well as after it. Two graphs are shown for the SW pulp gel in NaOH–ZnO. One of the graphs (turquoise) is taken from the swollen fiber part of the sample and the other one (violet) from between the swollen fibers. In addition, Fig. 5a shows the Raman graph of the amorphous cellulose prepared from the MCC. It should be noted that all of the graphs in Fig. 5 are normalized on the band at ca. 1096 cm^{-1} which is assigned to the glycosidic COC stretching and the so-called “ring breathing” of the cellulose chain (Schenzel and Fischer 2001; Wiley and Atalla 1987).

Interestingly, the graph of the MCC dissolved in the NaOH–ZnO system (red) in Fig. 5a resembles closely the one of the amorphous cellulose (black). Especially, the band observed for the MCC at ca. 380 cm^{-1} is missing from the graphs of the amorphous cellulose and the MCC dissolved in NaOH–ZnO (the position marked as a dashed line in the figure). This band is closely related to the crystallinity of cellulose, and in fact the ratio of the bands at 380 and 1096 cm^{-1} has been used to quantify cellulose I crystallinity (Agarwal et al. 2010). Moreover, the shape of the Raman graph of the MCC is typical to that of cellulose I while the graphs of the amorphous cellulose and the MCC

dissolved in the NaOH–ZnO resemble those ones reported earlier for amorphous cellulose and cellulose dissolved in $\text{ZnCl}_2 + 4\text{H}_2\text{O}$ (Agarwal 2014; Fischer et al. 2005; Schenzel and Fischer 2001). In the graph of the MCC in NaOH–ZnO the bands typical of cellulose in the regions 1000–1150 cm^{-1} and 1250–1500 cm^{-1} are broader than what is observed for cellulose I, the shoulder at 1120 cm^{-1} is missing, bands at ca. 1260 and 1460 cm^{-1} are observed and the band at ca. 899 cm^{-1} is stronger. The intensity of the band at ca. 899 cm^{-1} has been shown to be indirectly related to the crystallinity of cellulose (Li and Rennecker 2011) and the band at ca. 1460 cm^{-1} has been assigned to the scissor mode of the gg conformer of the CH_2OH group. The changes in the Raman profiles, especially the missing band at ca. 380 cm^{-1} , indicate that the crystalline network of cellulose has been destroyed when the MCC was dissolved in the NaOH–ZnO system. Similar changes in Raman graphs are also observed for cellosexaose dissolved in the NaOH–ZnO system (Fig. S4a in the Supplementary Material). However, a closer inspection of the graphs in Fig. 5a shows that there are also some differences between the graphs of the MCC in NaOH–ZnO and the amorphous cellulose. The band observed for the amorphous cellulose at 1260 cm^{-1} has shifted by almost 10 cm^{-1} to a higher wavenumber. This band is in a so-called transition region in which the vibrational modes involve significant amounts of skeletal stretching and methine bending vibrations whose frequency distributions are sensitive to the orientation of the glycosidic linkages (Schenzel and Fischer 2001). The other clear difference between the Raman graphs of

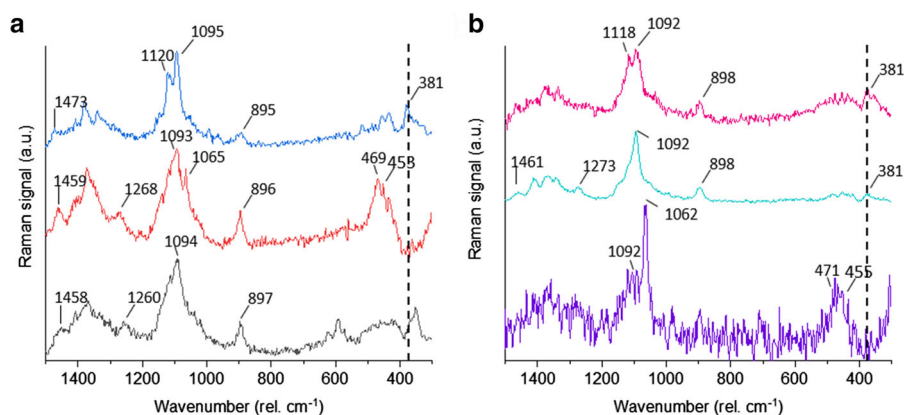


Fig. 5 Normalized Raman spectra of **a** MCC (top/blue), MCC in NaOH–ZnO (middle/red) and amorphous cellulose (bottom/black) and **b** SW pulp (top/pink), SW pulp in NaOH–ZnO (fiber) (middle/turquoise) and SW pulp in NaOH–ZnO (solution) (bottom/violet)

the MCC in NaOH–ZnO and the amorphous cellulose is found in the region $320\text{--}520\text{ cm}^{-1}$. The vibrational modes in this region are to a large extent delocalized and consist predominantly of skeletal bending vibrations of CCC, COC, OCC and OCO with small contribution of CCH, OCH methine bending as well as skeletal CC and CO stretching vibrations (Schenzel and Fischer 2001). The differences in this region indicate that the local environments of the individual cellulose chains are different in the NaOH–ZnO solvent system as compared to the amorphous cellulose. The bands in the graph of the MCC in NaOH–ZnO at ca. 1062 , 471 and 455 cm^{-1} originate from the NaOH–ZnO solvent and are also visible in the Raman graph of the pure solvent (Fig. S4b in the Supplementary Material).

The spectrum of the SW pulp (pink) in Fig. 5b is typical for bleached SW kraft pulp (Agarwal and Ralph 1997). In addition to cellulose, the Raman spectrum of the SW pulp includes the bands of hemicelluloses contained by the pulp. The Raman bands of hemicelluloses are broader and less intense than cellulose due to their less ordered structure, and, due to the chemical similarity between hemicelluloses and cellulose, their bands overlap with those ones of cellulose (Agarwal and Ralph 1997). Figure 5b contains also the normalized Raman spectrum of the swollen SW pulp fiber in the NaOH–ZnO solvent system (turquoise) as well as a spectrum taken of the area in between the swollen fibers in the gel (violet). The graph of the swollen fiber has a weak band at 381 cm^{-1} indicating that some amount of cellulose I crystallinity is left in the fiber. However, the shape of the spectrum in the $1000\text{--}1170\text{ cm}^{-1}$ region resembles that of cellulose II (Agarwal 2014; Schenzel and Fischer 2001) indicating that the sample has partly turned into this polymorph. Moreover, the band typical for amorphous cellulose at 1260 cm^{-1} has shifted by ca. 10 cm^{-1} to 1273 cm^{-1} and a band at ca. 1460 cm^{-1} appeared in the graph, the same phenomena that were observed for the MCC in NaOH–ZnO. The graph of the area in between the swollen fibers show bands originating from the solvent as well as weak and broad cellulose bands in the regions between $1000\text{--}1150\text{ cm}^{-1}$ and $1250\text{--}1500\text{ cm}^{-1}$ indicating that probably a small amount of cellulose has dissolved into the system. It should be noted that this graph had a low intensity overall which is shown by

the high signal-to-noise ratio of the normalized graph (violet) in Fig. 5b.

Based on the Raman spectra, it seems that the crystalline network of cellulose is destroyed when MCC is dissolved in the NaOH–ZnO system. However, the molecules are not able to take in any position in the solution but they are instead confined to certain positions, indicated for example by the appearance of the Raman bands in the region between 320 and 520 cm^{-1} which are missing from the spectrum of the amorphous cellulose. Moreover, the appearance of the band at ca. 1460 cm^{-1} indicates that the cellulose chains are confined to the gg conformer of the CH_2OH group. We suggest that in the NaOH–ZnO system the addition of ZnO aids the dissolution of cellulose and delays self-aggregation by coordinatively binding to the C2 and C3 OH groups of the cellulose chains deliberated from the crystalline structure and forming a metastable structure similar to the ring-structured complex, zinc glycerolate, formed in the reaction of ZnO and glycerol (Rémiás et al. 2009; Turney et al. 2013). The proposed structure is shown in Fig. 6. The formation of such a structure would disturb the conjugated electron system of the hydrogen bonded network of cellulose and thus aid in keeping the molecules apart from each other. However, the complex is not stable and gelation of cellulose might eventually happen. It has been shown for zinc glycerolate that the complex is not stable in aqueous environment and it is instead hydrolyzed over time at room temperature (Yee et al. 2012). In contrast to the MCC, the SW pulp did not dissolve well in the NaOH–ZnO system. For this sample, it was shown that the cellulose I crystalline structure of the swollen fiber

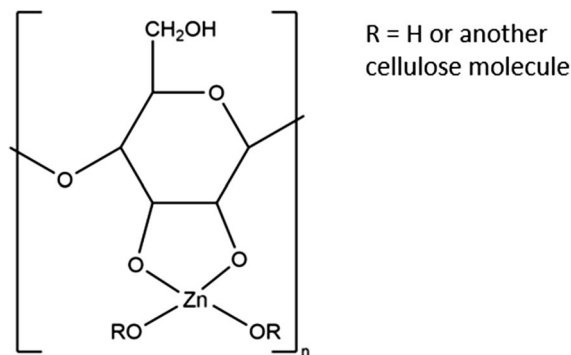


Fig. 6 Proposed structure for cellulose dissolved in the NaOH–ZnO system

was partly changed to cellulose II in NaOH–ZnO. According to the Raman spectroscopy, it is possible that some zinc oxide has bound to cellulose also in the case of this sample possibly forming the ring-structured complex as described above.

Conclusions

The addition of ZnO to aqueous NaOH aids the dissolution of cellulose and hinders its self-aggregation in solution. However, even with the addition of ZnO, a temperature below 0 °C is required to dissolve cellulose. Cellulose dissolution in aqueous NaOH at low temperature is generally explained by the formation of NaOH hydrates that are able to permeate into the cellulose network detaching individual chains from each other and forming a new network with it. It has been proposed that at the NaOH concentration optimal for cellulose dissolution (7–10%), an unstable equilibrium exists between NaOH hydrates bonded to each other and to cellulose. On the other hand, cellulose is in a dissociated form in the strongly alkaline environment which is also expected to enhance its dissolution due to charging up the polymer. We suggest that in this system, the addition of ZnO aids the dissolution of cellulose and delays its self-aggregation by coordinatively binding to the C2 and C3 OH groups of the cellulose chains deliberated from the crystalline structure and thus forming a ring-like structure similar to zinc glycerolate. The formation of this complex would disturb the conjugated electron system of the hydrogen bonded network of cellulose and thus aid in keeping the molecules apart from each other. Based on the Raman spectroscopic study as well as the TEMPO⁺-reactivity of the MCC in NaOH–ZnO it is clear that cellulose has dissolved completely in the NaOH–ZnO system. Moreover, based on the Raman spectra it is possible that a Zn-cellulose complex is formed when cellulose is dissolved in the NaOH–ZnO system and the formation of such a structure can explain the observed difference between the reactivities of MCC dissolved in aqueous NaOH–ZnO as compared to MCC dissolved in [Emim][Ac] and LiCl/DMAc. The formation of a metastable structure between cellulose and ZnO would slow down the recrystallization of cellulose when aqueous 4-AcNH-TEMPO⁺ is added into the system which is observed as the consumption of

4-AcNH-TEMPO⁺ over the whole reaction time as compared to the [Emim][Ac] and LiCl/DMAc systems in which the consumption of 4-AcNH-TEMPO⁺ levels off in the beginning of the reaction as cellulose is recrystallizing. The SW pulp with a high DP dissolved poorly in the NaOH–ZnO system and it was partially swollen and turned into cellulose II. Based on the Raman data, it is possible that a Zn-cellulose complex has also formed in this sample.

Acknowledgments This work was a part of a joint research project between UPM-Kymmene Oyj and Aalto University. The authors would like to thank the research team for the fruitful discussions at the project meetings. Moreover, the authors would like to acknowledge the financial support from the Association of the Forest Product Engineers (PI) and we are grateful for the support by the FinnCERES Materials Bioeconomy Ecosystem. Finally, we would like to give a special thank you to Dr Arno Parviainen for preparing the amorphous cellulose sample in the Laboratory of Organic Chemistry at the University of Helsinki, Dr Pegah Khanjani for instructing with the TEMPO⁺-reactivity measurements and Mrs Rita Hatakka for her assistance with the GPC/SEC and HPAEC measurements. This work made use of the Aalto University Bioeconomy facilities as well as the Aalto University Nanomicroscopy Center (Aalto NMC) facilities.

Funding This work was a part of a joint research project between UPM-Kymmene Oyj and Aalto University. In addition, the authors would like to acknowledge the financial support from the Association of the Forest Product Engineers (PI) and the FinnCERES Materials Bioeconomy Ecosystem.

Availability of data and material The data that support the findings of this study are available from the corresponding author upon reasonable request.

Compliance with ethical standards

Conflict of interest The authors declare that they have no conflict of interest.

Open Access This article is licensed under a Creative Commons Attribution 4.0 International License, which permits use, sharing, adaptation, distribution and reproduction in any medium or format, as long as you give appropriate credit to the original author(s) and the source, provide a link to the Creative Commons licence, and indicate if changes were made. The images or other third party material in this article are included in the article's Creative Commons licence, unless indicated otherwise in a credit line to the material. If material is not included in the article's Creative Commons licence and your intended use is not permitted by statutory regulation or exceeds the permitted use, you will need to obtain permission directly from the copyright holder. To view a copy of this licence, visit <http://creativecommons.org/licenses/by/4.0/>.

References

- Agarwal UP (2014) 1064 nm FT-Raman spectroscopy for investigations of plant cell walls and other biomass materials. *Front Plant Sci* 5:1–12. <https://doi.org/10.3389/fpls.2014.00490>
- Agarwal UP (2019) Analysis of cellulose and lignocellulose materials by Raman spectroscopy: a review of the current status. *Molecules* 24:1659–1675. <https://doi.org/10.3390/molecules24091659>
- Agarwal UP, Ralph SA (1997) FT-Raman spectroscopy of wood: identifying contributions of lignin and carbohydrate polymers in the spectrum of black spruce (*Picea mariana*). *Appl Spectrosc* 51:1648–1655. <https://doi.org/10.1366/0003702971939316>
- Agarwal UP, Reiner RS, Ralph SA (2010) Cellulose I crystallinity determination using FT-Raman spectroscopy: univariate and multivariate methods. *Cellulose* 17:721–733. <https://doi.org/10.1007/s10570-010-9420-z>
- Alves I, Medronho B, Antunes FE, Topgaard D, Lindman B (2016) Dissolution state of cellulose in aqueous systems. I. Alkaline solvents. *Cellulose* 23:247–258. <https://doi.org/10.1007/s10570-015-0809-6>
- Bialik E, Stenqvist B, Fang Y, Östlund Å, Furó I, Lindman B, Lund M, Bernin D (2016) Ionization of cellobiose in aqueous alkali and the mechanism of cellulose dissolution. *J Phys Chem Lett* 7:5044–5048. <https://doi.org/10.1021/acs.jpcl.6b02346>
- Bichsel Y, von Gunten U (1999) Determination of iodide and iodate by ion chromatography with postcolumn reaction and UV/visible detection. *Anal Chem* 71:34–38. <https://doi.org/10.1021/ac980658j>
- Blackwell J, Vasko PD, Koenig JL (1970) Infrared and Raman spectra of the cellulose from the cell wall of *Valonia ventricosa*. *J Appl Phys* 41:4375–4379. <https://doi.org/10.1063/1.1658470>
- Borrega M, Tolonen LK, Bardot F, Testova L, Sixta H (2013) Potential of hot water extraction of birch wood to produce high-purity dissolving pulp after alkaline pulping. *Bioresour Technol* 135:665–671. <https://doi.org/10.1016/j.biortech.2012.11.107>
- Budtova T, Navard P (2016) Cellulose in NaOH–water based solvents: a review. *Cellulose* 23:5–55. <https://doi.org/10.1007/s10570-015-0779-8>
- Cai J, Zhang L, Liu S, Liu Y, Xu X, Chen X, Chu B, Guo X, Xu J, Cheng H, Han CC, Kuga S (2008) Dynamic self-assembly induced rapid dissolution of cellulose at low temperatures. *Macromolecules* 41:9345–9351. <https://doi.org/10.1021/ma801110g>
- Davidson GF (1934) The dissolution of chemically modified cotton cellulose in alkaline solutions. Part I: in solutions of sodium hydroxide, particularly at temperatures below the normal. *J Text Inst* 25:T174–T196. <https://doi.org/10.1080/19447023408661621>
- Davidson GF (1936) The dissolution of chemically modified cotton cellulose in alkaline solutions. Part II: a comparison of the solvent action of solutions of lithium, sodium, potassium and tetramethylammonium hydroxides. *J Text Inst* 27:T112–T130. <https://doi.org/10.1080/19447023608661674>
- De Nooy AEJ, Besemer AC, van Bekkum H (1994) Highly selective tempo mediated oxidation of primary alcohol groups in polysaccharides. *Recl Trav Chim Pays-Bas* 113:165–166. <https://doi.org/10.1002/recl.19941130307>
- Egal M, Budtova T, Navard P (2007) Structure of aqueous solutions of microcrystalline cellulose/sodium hydroxide below 0 °C and the limit of cellulose dissolution. *Biomacromol* 8:2282–2287. <https://doi.org/10.1021/bm0702399>
- Eronen P, Österberg M, Jääskeläinen A-S (2009) Effect of alkaline treatment on cellulose supramolecular structure studied with combined confocal Raman spectroscopy and atomic force microscopy. *Cellulose* 16:167–178. <https://doi.org/10.1007/s10570-008-9259-8>
- Fischer S, Schenzel K, Fischer K, Diepenbrock W (2005) Applications of FT Raman spectroscopy and micro spectroscopy characterizing cellulose and cellulosic biomaterials. *Macromol Symp* 223:41–56. <https://doi.org/10.1002/masy.200550503>
- Gericke M, Trygg J, Fardim P (2013) Functional cellulose beads: preparation, characterization and applications. *Chem Rev* 113:4812–4836. <https://doi.org/10.1021/cr300242j>
- Ghasemi M, Alexandridis P, Tsianou M (2017a) Cellulose dissolution: insights on the contributions of solvent-induced decrystallization and chain disentanglement. *Cellulose* 24:571–590. <https://doi.org/10.1007/s10570-016-1145-1>
- Ghasemi M, Tsianou M, Alexandridis P (2017b) Assessment of solvents for cellulose dissolution. *Bioresour Technol* 228:330–338. <https://doi.org/10.1016/j.biortech.2016.12.049>
- Hagman J, Gentile L, Jessen CM, Behrens M, Bergqvist K-E, Olsson U (2017) On the dissolution state of cellulose in cold alkali solutions. *Cellulose* 24:2003–2015. <https://doi.org/10.1007/s10570-017-1272-3>
- Heinze T, Dicke R, Koschella A, Kull AH, Klotz E-A, Koch W (2000) Effective preparation of cellulose derivatives in a new simple cellulose solvent. *Macromol Chem Phys* 201:627–631. [https://doi.org/10.1002/\(SICI\)1521-3935\(20000301\)201:6%3c627:AID-MACP627%3e3.0.CO;2-Y](https://doi.org/10.1002/(SICI)1521-3935(20000301)201:6%3c627:AID-MACP627%3e3.0.CO;2-Y)
- Huh E, Yang J-H, Lee C-H, Ahn I-S, Mhin BJ (2020) Thermodynamic analysis of cellulose complex in NaOH–urea solution using reference interaction site model. *Cellulose*. <https://doi.org/10.1007/s10570-020-03202-w>
- Isogai A, Atalla RH (1998) Dissolution of cellulose in aqueous NaOH solutions. *Cellulose* 5:309–319. <https://doi.org/10.1023/A:1009272632367>
- Isogai A, Saito T, Fukuzumi H (2011) TEMPO-oxidized cellulose nanofibers. *Nanoscale* 3:71–85. <https://doi.org/10.1039/C0NR00583E>
- Janson J (1970) Calculation of the polysaccharide composition of wood and pulp. *Pap Puu* 52:323–329
- Khanjani P, Väisänen S, Lovikka V, Nieminen K, Maloney T (2017) Assessing the reactivity of cellulose by oxidation with 4-acetamido-2,2,6,6-tetramethylpiperidine-1-oxo-piperidinium cation under mild conditions. *Carbohydr Polym* 176:293–298. <https://doi.org/10.1016/j.carbpol.2017.08.092>

- Kihlman M, Medronho BF, Romano AL, Germgård U, Lindman B (2013) Cellulose dissolution in an alkali based solvent: influence of additives and pretreatments. *J Braz Chem Soc* 24:295–303. <https://doi.org/10.5935/0103-5053.20130038>
- Li Q, Renneckar S (2011) Supramolecular structure characterization of molecularly thin cellulose I nanoparticles. *Biomacromol* 12:650–659. <https://doi.org/10.1021/bm101315y>
- Lindman B, Karlström G, Stigsson L (2010) On the mechanism of dissolution of cellulose. *J Mol Liq* 156:76–81. <https://doi.org/10.1016/j.molliq.2010.04.016>
- Liu W, Budtova T, Navard P (2011) Influence of ZnO on the properties of dilute and semi-dilute cellulose–NaOH–water solutions. *Cellulose* 18:911–920. <https://doi.org/10.1007/s10570-011-9552-9>
- Lovikka V, Khanjani P, Väisänen S, Vuorinen T, Maloney TC (2016) Porosity of wood pulp fibers in the wet and highly open dry state. *Micropor Mesopor Mat* 234:326–335. <https://doi.org/10.1016/j.micromeso.2016.07.032>
- Lu A, Liu Y, Zhang L, Potthast A (2011) Investigation of metastable solution of cellulose dissolved in NaOH/urea aqueous system at low temperature. *J Phys Chem B* 115:12801–12808. <https://doi.org/10.1021/jp206643f>
- Medronho B, Lindman B (2014) Competing forces during cellulose dissolution: from solvents to mechanisms. *Curr Opin Colloid In* 19:32–40. <https://doi.org/10.1016/j.cocis.2013.12.001>
- Medronho B, Lindman B (2015) Brief overview on cellulose dissolution and regeneration interactions and mechanisms. *Adv Colloid Interfac* 222:502–508. <https://doi.org/10.1016/j.cis.2014.05.004>
- Mormann W, Wezstein M (2009) Trimethylsilylation of cellulose in ionic liquids. *Macromol Biosci* 9:369–375. <https://doi.org/10.1002/mabi.200800192>
- Okita Y, Saito T, Isogai A (2010) Entire surface oxidation of various cellulose microfibrils by TEMPO-mediated oxidation. *Biomacromol* 11:1696–1700. <https://doi.org/10.1021/bm100214b>
- Pääkkönen T, Bertinetto C, Pönni R, Tummala GK, Nuopponen M, Vuorinen T (2015) Rate-limiting steps in bromide-free TEMPO-mediated oxidation of cellulose: quantification of the N-oxoammonium cation by iodometric titration and UV–Vis spectroscopy. *Appl Catal A* 505:532–538. <https://doi.org/10.1016/j.apcata.2015.07.024>
- Pereira A, Duarte H, Nosrati P, Gubitosi M, Gentile L, Romano A, Medronho B, Olsson U (2018) Cellulose gelation in NaOH solutions is due to cellulose crystallization. *Cellulose* 25:3205–3210. <https://doi.org/10.1007/s10570-018-1794-3>
- Rabideau BD, Agarwal A, Ismail AE (2013) Observed mechanism for the breakup of small bundles of cellulose I α and I β in ionic liquids from molecular dynamics simulations. *J Phys Chem B* 117:3469–3479. <https://doi.org/10.1021/jp310225t>
- Rémiás R, Kukovec Á, Darányi M, Kozma G, Varga S, Kónya Z, Kiricsi I (2009) Synthesis of zinc glycerolate microstacks from a ZnO nanorod sacrificial template. *Eur J Inorg Chem*. <https://doi.org/10.1002/ejic.200900308>
- Roy C, Budtova T, Navard P (2003) Rheological properties and gelation of aqueous cellulose–NaOH solutions. *Biomacromol* 4:259–264. <https://doi.org/10.1021/bm020100s>
- Saito T, Kimura S, Nishiyama Y, Isogai A (2007) Cellulose nanofibers prepared by TEMPO-mediated oxidation of native cellulose. *Biomacromol* 8:2485–2491. <https://doi.org/10.1021/bm0703970>
- Saito T, Hirota M, Tamura N, Kimura S, Fukuzumi H, Heux L, Isogai A (2009) Individualization of nano-sized plant cellulose fibrils by direct surface carboxylation using TEMPO catalyst under neutral conditions. *Biomacromol* 10:1992–1996. <https://doi.org/10.1021/bm900414t>
- Salminen R, Reza M, Pääkkönen T, Peyre J, Kontturi E (2017) TEMPO-mediated oxidation of microcrystalline cellulose: limiting factors for cellulose nanocrystal yield. *Cellulose* 24:1657–1667. <https://doi.org/10.1007/s10570-017-1228-7>
- Schenzel K, Fischer S (2001) NIR FT Raman spectroscopy: a rapid analytical tool for detecting the transformation of cellulose polymorphs. *Cellulose* 8:49–57. <https://doi.org/10.1023/A:1016616920539>
- Sluiter A, Hames B, Ruiz R, Scarlata C, Sluiter J, Templeton D, Crocker D (2008) Determination of structural carbohydrates and lignin in biomass. In: DOE (ed) National renewable energy laboratory. Technical report: NREL/TP-510-42618
- Turney TW, Patti A, Gates W, Shaheen U, Kulasegaram S (2013) Formation of glycerol carbonate from glycerol and urea catalyzed by metal monoglycerolates. *Green Chem* 15:1925–1931. <https://doi.org/10.1039/C3GC37028C>
- Wang S, Lu A, Zhang L (2016) Recent advances in regenerated cellulose materials. *Prog Polym Sci* 53:169–206. <https://doi.org/10.1016/j.progpolymsci.2015.07.003>
- Wawro D, Stęplewski W, Bodek A (2009) Manufacture of cellulose fibres from alkaline solutions of hydrothermally-treated cellulose pulp. *Fibres Text East Eur* 17:18–22
- Wiley JH, Atalla RH (1987) Band assignments in the Raman spectra of celluloses. *Carbohydr Res* 160:113–129
- Yang Q, Fukuzumi H, Saito T, Isogai A, Zhang L (2011a) Transparent cellulose films with high gas barrier properties fabricated from aqueous alkali/urea solutions. *Biomacromol* 12:2766–2771. <https://doi.org/10.1021/bm200766v>
- Yang Q, Qi H, Lue A, Hu K, Cheng G, Zhang L (2011b) Role of sodium zincate on cellulose dissolution in NaOH/urea aqueous solution at low temperature. *Carbohydr Polym* 83:1185–1191. <https://doi.org/10.1016/j.carbpol.2010.09.020>
- Yee CM, Hassan HA, Hassan ZAA, Ismail R (2012) Zinc glycerolate: potential active for topical application. *J Oil Palm Res* 24:1287–1295

Publisher's Note Springer Nature remains neutral with regard to jurisdictional claims in published maps and institutional affiliations.